

# RL-MUL: Multiplier Design Optimization with Deep Reinforcement Learning

Dongsheng Zuo\*, Jiadong Zhu\*, Yikang Ouyang, Yuzhe Ma

**Abstract**—Multiplication is a fundamental operation in many applications, and multipliers are widely adopted in various circuits. However, optimizing multipliers is challenging and non-trivial due to the huge design space. In this paper, we propose RL-MUL, a multiplier design optimization framework based on reinforcement learning. Specifically, we utilize matrix and tensor representations for the compressor tree of a multiplier, based on which the convolutional neural networks can be seamlessly incorporated as the agent network. The agent can learn to optimize the multiplier structure based on a Pareto-driven reward which is customized to accommodate the trade-off between area and delay. Additionally, the capability of RL-MUL is extended to optimize the fused multiply-accumulator (MAC) designs. Experiments are conducted on different bit widths of multipliers. The results demonstrate that the multipliers produced by RL-MUL can dominate all baseline designs in terms of area and delay. The performance gain of RL-MUL is further validated by comparing the area and delay of processing element arrays using multipliers from RL-MUL and baseline approaches.

## I. INTRODUCTION

In the era of rapid advancements in neural networks and streaming media applications, the demand for computational power has intensified. Notably, the multiply-accumulate (MAC) computation can constitute over 99% of operations in standard deep neural networks, as shown in Fig. 1. At the hardware layer, multipliers and MAC circuits are integral to the architecture of compute-intensive circuits, significantly impacting the system performance, energy consumption, spatial requirements, and design complexities. Therefore, swiftly designing multipliers and MACs that meet metric specifications such as power, performance, and area (PPA) becomes imperative.

Multiplier design optimization is non-trivial due to the huge design space. The multiplier design is fundamentally segmented into three primary components: a partial product generator (PPG), a compressor tree (CT), and a carry propagation adder (CPA). Among these, the optimization of the Compressor Tree (CT) is pivotal, as it significantly influences the PPA of a multiplier. The architecture of the compressor tree was first introduced in [1], designed for parallel compression (i.e., addition) of partial products in multiplication

The preliminary version has been presented at the ACM/IEEE Design Automation Conference (DAC) in 2023. This work is supported in part by the Guangzhou-HKUST(GZ) Joint Funding Program (No. 2023A03J0155) and Guangzhou Municipal Science and Technology Project (Municipal Key Laboratory Construction Project, Grant No.2023A03J0013). (Corresponding authors: Yuzhe Ma)

\*D. Zuo and J. Zhu contribute equally to this work.

D. Zuo, J. Zhu, Y. Ouyang, Y. Ma are with the Microelectronics Thrust of The Hong Kong University of Science and Technology (Guangzhou), Guangzhou, China.

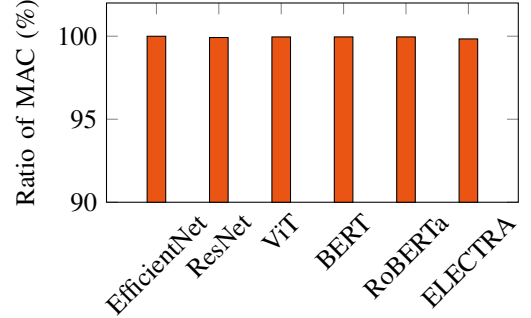


Fig. 1 Ratios of MAC computations in various neural networks.

operations. This innovation has enabled the application of compressor trees in other datapath circuits, such as MACs and vector adders. Conventionally, MAC operations extend the functionality of multipliers by incorporating an accumulator after multiplication, resulting in increased operational delay. In contrast, the merged MAC is proposed, which enables the execution of MAC operations within the multiplication time by integrating the addend directly into the partial products [2]. This approach also allows the optimization methodologies developed for multipliers to be applied to MAC design optimization. Generally, datapath designs, including adders, multipliers, and MACs, can be completed manually. Take multiplier design as an example. The manual design includes Wallace tree structure [1], Dadda tree structure [3], and further optimized designs based on them [4]–[7], which effectively optimize area, power, and performance for specific technology nodes and applications. The Wallace tree strategically organized the compressor layers [4]. An area-reduced tree is proposed by using a maximum number of 3:2 compressors early and carefully placing 2:2 compressors [6]. Itoh *et al.* [5] proposed an advanced rectangular-styled tree structure, tailored specifically for 32-bit  $\times$  24-bit multipliers. Optimizations for merged MAC structures have been explored based on the characteristics of multiply-accumulate operations. Tung *et al.* [8] proposed a method where the final addition and accumulation of higher significance bits are merged to the partial products of the next multiplication operation. Zhang *et al.* [9] proposed a strategy optimizing pipeline merged MAC. These regular structure-based designs may not always meet the stringent PPA specifications required. To address this, full custom-designed multipliers are developed, which are finely optimized for specific fabrication processes or unique application scenarios [10]–[12]. However, it is obvious that

a significant engineering effort is required to explore the huge design space with manual design, which limits design flexibility and efficiency.

The automatic generation or search methods have provided a more flexible solution to datapath designs. A three-dimensional method for designing the compressor tree was proposed, which utilized an input-to-output delay model [13]–[15]. Integer linear programming (ILP) is another widely investigated approach for datapath circuit optimization. Xiao *et al.* [16] employed ILP for global optimization of multiplier design by minimizing the total number of compressors in the compressor tree. In addition, ILP has also been applied for exploring adder trees based on analytical area, power, and timing models [17]. However, these works may suffer from the long runtime of the ILP solver as well as the misaligned objective between the modeled PPA metrics and real synthesized metrics. Heuristic search strategies utilize various pruning techniques and avoid exhaustive searches [18]–[22]. A heuristic is introduced in [20] for the design of compressor trees using generalized parallel counters (GPCs), aiming to optimize the balance between logic utilization and delay. Kumm *et al.* [22] further advanced heuristic method in [20], [21] and combined the heuristic method with ILP.

Recently machine learning methodologies have become promising solutions for circuit optimization and design space exploration, where various learning models are leveraged as surrogate models to evaluate designs during the search or optimization process [23]–[25]. An active learning-based prefix adder exploration framework is proposed in [24], which uses the Gaussian process regression model to predict the delay and area based on the feature extracted from the prefix tree structure. Geng *et al.* [23] further facilitated automatic feature learning for prefix adder structures and deployed a sequential optimization framework that employs the graph neural process as a surrogate model, which enables a more efficient and effective adder structure exploration. However, the exploration still highly relies on a regression model as a proxy to the real PPA, whose modeling accuracy significantly affects the final results. Contrary to existing approaches, reinforcement learning (RL) integrates actual PPA evaluations directly into its optimization loop, demonstrating its feasibility by efficiently navigating complex design spaces. Recent advancements have seen RL tackle a variety of challenges within electronic design automation (EDA), as evidenced by applications across different domains [25]–[27]. Given the complexity of multiplier design and the vastness of its design space, the feasibility of reinforcement learning in multiplier design optimization is underscored. RL addresses this gap by leveraging real synthesized metrics as rewards, enabling the identification and optimization of designs that perform better after synthesis. This method not only navigates through the expansive design space more effectively but also ensures the realization of more efficient and optimized circuit designs. In addition, RL algorithms can also be enhanced with parallelism by implementing different environment instances. By utilizing multiple threads, the stability and efficiency of deep reinforcement learning algorithms are enhanced.

In this manuscript, we propose an RL-based framework,

RL-MUL, which is tailored for the optimization of multipliers and merged MACs. It is non-trivial to obtain a suitable representation of the multiplier structure. To address this, we propose a matrix and a tensor representation for the compressor tree structures, based on which the convolutional neural networks can be seamlessly incorporated as the agent network in the RL environment. The agent can learn to make good moves based on a Pareto-driven reward which is customized to accommodate the trade-off between area and delay. To exploit the huge design space more efficiently, we prune the design space and leverage parallel RL optimization. To validate the effectiveness, RL-MUL is applied to design and optimize different bit widths of multipliers, which can outperform various baseline designs from different methods, including legacy designs, evolutionary algorithms, and integer linear programming. Furthermore, to validate the effectiveness of the optimized multipliers and MACs, a computation module, e.g., a process element (PE) array, is implemented with the multipliers and MACs generated by RL-MUL, and the PPA gets improved accordingly. In summary, the contributions are as follows:

- We propose RL-MUL, a multiplier optimization framework based on reinforcement learning, marking the first instance of applying reinforcement learning for this purpose to our knowledge.
- We present a matrix and a tensor representation for multipliers, which enables the seamless integration of deep neural networks as the agent network. A Pareto-driven reward is employed to accommodate the trade-off between the area and delay so that the agent can learn to achieve Pareto-optimal designs.
- To improve search efficiency within this framework, we further enhance the RL-MUL with a parallel training methodology to enable faster and more stable training.
- We broaden the scope of RL-MUL to include fused MAC to validate the applicability of the framework.
- Experimental results demonstrate that the multipliers and MACs produced by RL-MUL dominate all baseline designs in terms of both area and delay. Furthermore, applying the optimized multipliers and MACs to the implementation of a larger computation module also results in PPA improvement, which validates the effectiveness of the optimized designs.

## II. PRELIMINARY

### A. Multiplier Architecture

The multiplier typically comprises three primary components: a partial product generator (PPG), a compressor tree (CT), and a carry propagation adder, as shown in Fig. 2. PPG generates partial products (PPs) from the multiplicand and multiplier, while the CT compresses these PPs into two parallel rows. Subsequently, an adder is utilized to aggregate these two rows of PPs, culminating in the final product. A typical partial product generator generally employs  $N^2$  AND gates for an  $N$ -bit multiplier. A CT has multiple compression stages to compress the PPs into two rows. Predominantly, there are 3:2 compressors and 2:2 compressors, implemented

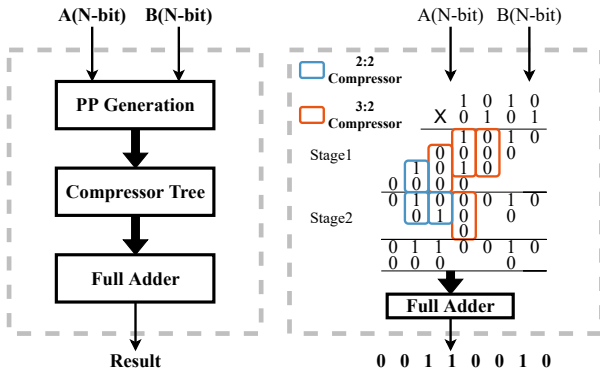


Fig. 2 Multiplier architecture

through a full adder and a half adder, respectively. A 3:2 (resp. 2:2) compressor applied at column  $j$  of stage  $i$  receives 3 (resp. 2) partial products as input from column  $j$  of stage  $i$ , passing the *sum* output to column  $j$  of stage  $i + 1$ , and the *carry out* to column  $j + 1$  of stage  $i + 1$ . Consequently, a 3:2 compressor decreases the partial products of column  $j$  by two, while a 2:2 compressor reduces them by one, each incrementing the partial products in column  $j + 1$  by one.

### B. Q-Learning

RL encompasses a collection of optimization problems referred to as *state*  $s$ , with a corresponding set of *actions*  $A$ . An agent transitions from one state  $s$  to another state  $s'$  by executing an action  $a \in A$ , consequently receiving a *reward*  $r(s, a)$  as an evaluation from the RL environment. The model governing action selection is known as the *policy*  $\pi$ . The primary objective of the RL agent is to devise a policy that optimizes the cumulative reward.

Q-learning is an RL algorithm that learns the scores of each action  $a$  for a given state  $s$ , and the score is called Q-value, represented by  $Q(s, a)$ . According to Bellman equation [28], the Q-value is calculated as follows:

$$Q(s, a) = r(s, a) + \gamma \max_{a'} Q(s', a'), \quad (1)$$

where  $s'$  indicates the next state, and  $\gamma$  is the discount factor. Therefore, the Q-value is updated by:

$$Q(s, a) = Q(s, a) + \alpha \left[ r(s, a) + \gamma \max_{a'} Q(s', a') - Q(s, a) \right], \quad (2)$$

where  $\alpha$  is the learning rate. In this paper, we utilize the deep Q-learning approach, leveraging a deep neural network to approximate the Q-value. Here, the state  $s$  represents the architecture of the multiplier, detailed in Section III-B. An action  $a$  alters the current multiplier architecture into a new one, effectively progressing to the next state. The reward  $r$  is quantified by the enhancements in the multiplier's area and delay metrics.

### C. Advantage Actor-Critic

The A2C algorithm [29] addresses the challenges of high variance and unstable learning due to strong correlations

between consecutive states by splitting the traditional RL model into two components: an actor that enacts policies and a critic that evaluates these actions. A policy network  $\pi(a|s; \theta)$  and a value network  $v(s; w)$  are employed, where  $\theta$  and  $w$  are the parameters of two neural networks, respectively. The synchronous multi-thread coordination method in A2C ensures uniform learning and parameter updates, significantly speeding up and stabilizing the training process [30]. The A2C algorithm employs bootstrapped advantage estimates generated by the critic instead of mere state-value approximations to enhance gradient estimation accuracy and learning efficiency [31]. With state  $s$  and action  $a$ , The advantage is defined as:

$$\hat{A}(s, a) = Q_\pi(s, a) - V_\pi(s), \quad (3)$$

where  $Q_\pi(s, a)$  indicates the action-value function that estimates the expected reward that can be obtained by taking action  $a$  and then following strategy  $\pi$  at state  $s$ , while  $V_\pi(s)$  indicates the state-value function that estimates the expected reward that can be obtained in state  $s$  if the strategy  $\pi$  is followed from that state instead of taking a specific action [30], [32].

For a known transition  $(s_t, a_t, r_t, s_{t+1})$ , to facilitate calculations of advantage function, we use a value network  $v(s_t; w)$  to approximate the state-value function  $V_\pi(s_t)$ , and estimate  $Q_\pi(s_t, a_t)$  through Monte Carlo methods based on the Bellman equation. Consequently, we can approximate (3) as:

$$\hat{A}(s_t, a_t) \approx r_t + \gamma \cdot v(s_{t+1}; w) - v(s_t; w), \quad (4)$$

where  $\gamma$  is the discount factor.

## III. PROPOSED METHOD

### A. Overview

As illustrated in Fig. 3, our framework leverages a reinforcement learning approach for multiplier design optimization. An RL agent engages in iterative interactions with its environment from an initial state  $s_0$ . At any given state  $s_t$ , the RL-MUL agent, guided by a policy  $\pi$  derived from the policy network, selects an action  $a_t$  from a set of legal actions. This action modifies the current multiplier configuration, leading to a new state  $s_{t+1}$ . Subsequently, a reward  $r_t$  is computed using EDA tools, facilitating the neural network model's update based on the received feedback.

### B. Multiplier Representation

The state space of the RL, denoted as  $\mathcal{S}$ , consists of all possible configurations of  $N$ -bit multipliers. We recognize the count of various compressors in each column as a critical attribute influencing the synthesized performance metrics of the multipliers. Consequently, we characterize the multiplier architecture using the aggregate counts of 3:2 and 2:2 compressors across columns, encapsulated by a matrix  $\mathbf{M} \in \mathbb{R}^{2N \times 2}$ . In this matrix, the first and second rows quantify the total 3:2 and 2:2 compressors in each column, respectively. An illustration of a 4-bit multiplier structure alongside its matrix representation  $\mathbf{M}$  is provided in Fig. 4. To derive a complete multiplier structure from  $\mathbf{M}$ , the compressors are

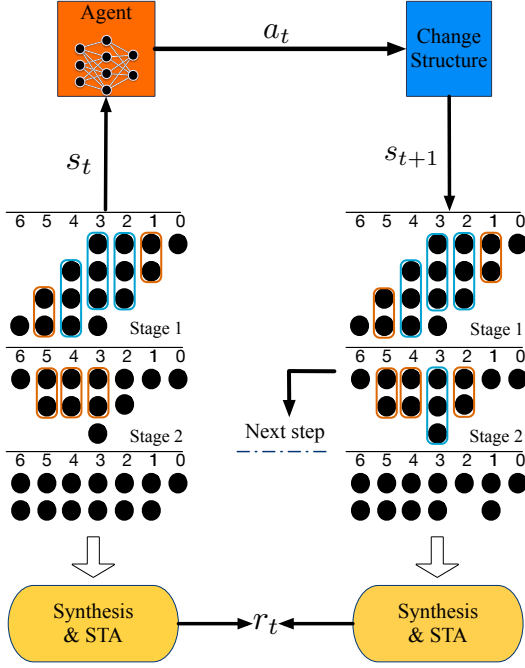


Fig. 3 RL-based multiplier optimization framework

allocated to specific stages. However, the mapping from  $M$  to the structures is not unique since different assignments of compressors in multiple stages may have the same overall number in each column. To achieve a distinctive representation, we advance to a tensor representation that offers more informative insights, as illustrated in Fig. 4.

We represent the tensor as  $\mathcal{T} \in \mathbb{R}^{K \times 2N \times ST}$ , with  $K$  indicating the total kinds of compressors used and  $ST$  the stage count. Specifically, we utilize 3:2 and 2:2 compressors, thus  $K = 2$ . This framework is designed for potential extension to accommodate more compressor variants. The tensors  $\mathbf{T}^{(0)} = \mathcal{T}_{0,:,:} \in \mathbb{R}^{2N \times ST}$  and  $\mathbf{T}^{(1)} = \mathcal{T}_{1,:,:} \in \mathbb{R}^{2N \times ST}$  respectively map the placement of 3:2 and 2:2 compressors. The elements  $t_{ij}^{(0)}$  and  $t_{ij}^{(1)}$  denote the quantity of 3:2 and 2:2 compressors at the  $j$ -th column of the  $i$ -th stage. Given a matrix  $M$  that contains the information of the overall number of compressors in each column, we can construct the tensor representation  $\mathcal{T}$  correspondingly based on an assignment scheme of the compressors in different stages.

For the assignment process, we employ a deterministic method that assigns compressors from the least to the most significant bit columns, prioritizing 3:2 compressors and then utilizing 2:2 compressors where applicable. This method progresses through stages until all compressors are allocated, as detailed in Algorithm 1. This approach guarantees a unique tensor representation for each multiplier structure, facilitating precise and unambiguous characterizations of the multiplier architecture.

### C. Extend to Merged Multiply-Accumulator Architecture

An integral component of many digital signal processing systems and neural network architectures is the multiply accumulator (MAC), which can be a decisive factor in deter-

### Algorithm 1 Compressor Assignment

**Require:**  $M$ : Matrix representation

**Ensure:**  $\mathcal{T}$ : Tensor representation.

```

1: for  $j \leftarrow 1$  to  $2N$  do
2:    $i \leftarrow 0$ 
3:   while column  $j$  exists not assigned comp. do
4:     Assign 3:2 comp. to stage  $i$  column  $j$  first
5:     Update  $t_{ij}^{(0)}$  in  $\mathbf{T}^{(0)}$ 
6:     if Remaining PPs  $\geq 2$  then
7:       Assign 2:2 comp. to stage  $i$  column  $j$ 
8:       Update  $t_{ij}^{(1)}$  in  $\mathbf{T}^{(1)}$ 
9:     end if
10:     $i \leftarrow i + 1$ 
11:  end while
12: end for
13:  $\mathcal{T}_{0,:,:} \leftarrow \mathbf{T}^{(0)}$ 
14:  $\mathcal{T}_{1,:,:} \leftarrow \mathbf{T}^{(1)}$ 

```

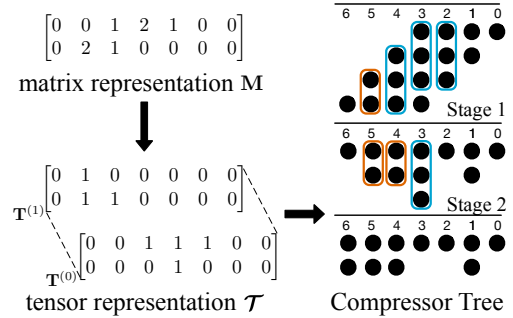


Fig. 4 Structure representation.

mining the overall performance of many computing-intensive systems. Incorporating compressor trees within MACs offers a pathway to enhance their efficiency. Rather than treating multiplication and accumulation as sequential operations, this approach seamlessly integrates them. By merging the accumulation (addition) directly into the partial product stages of multiplication and conducting partial product compression, we can capitalize on parallelism, thus potentially speeding up the entire MAC operation. We can see that the proposed RL-MUL framework can seamlessly support the optimization of fused MAC design.

By integrating the addition into the partial product generation phase, the representation within RL-MUL is tweaked to consider the intricacies of the MAC operation. The aim is to train the RL agent to explore and design optimal MAC structures, utilizing compressor trees for efficient parallel addition. Therefore, the representations in Section III-B can be easily extended to MACs by providing “merged” partial products, and the training procedure will be identical. In Section V, we will demonstrate the effectiveness and superiority of the RL-MUL for fused MAC design.

### D. Multiplier Modification

In the RL agent’s context, an action  $a$  signifies the agent’s choice to alter the existing structure of the multiplier. The

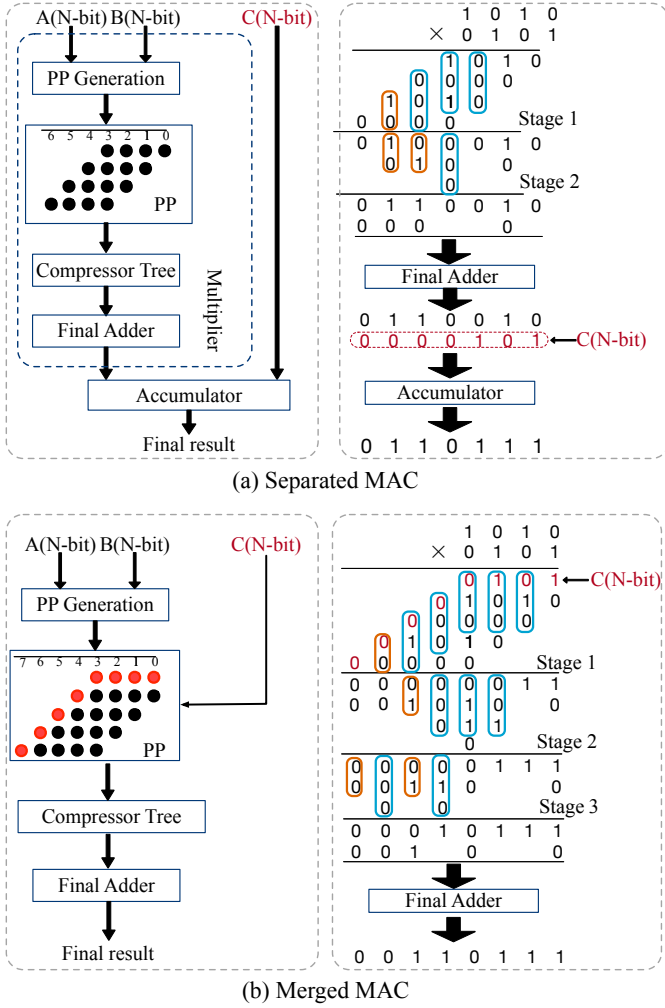


Fig. 5 MAC architectures

agent can choose from four distinct actions for each column: adding or removing a 2:2 compressor, and replacing a 3:2 or a 2:2 compressor with another type. We denote  $res_j$  to present the PP number after compression of column  $j$ , which should only be 1 or 2. Actions leading to  $res_j$  values of 0 or 3, such as adding or removing a 3:2 compressor, are excluded, thereby defining the action space as  $|A| = 2N \times 4 = 8N$ . It is important to note that not every action is feasible to yield a legal multiplier structure instantly. For instance, if there is no 2:2 compressor in column 1 as depicted in Fig. 4, attempting to remove a 2:2 compressor from this column is considered invalid. Similarly, any action  $a$  on column  $j$  that results in the partial product (PP) numbers post-compression being either 0 or 3 would be considered invalid. Take another example from Fig. 4. Removing a 2:2 compressor from column 4 would lead to  $res_4$  equating to three, thereby invalidating the action.

For a compressor tree with  $2N$  columns, the output of a deep Q-network is a vector that indicates the predicted Q-values:

$$Q(s_t) = [q_{11}, q_{12}, q_{13}, q_{14}, \dots, q_{2N,1}, q_{2N,2}, q_{2N,3}, q_{2N,4}], \quad (5)$$

where each group of  $q_{j1}, q_{j2}, q_{j3}, q_{j4}$  indicates the Q-value of the four actions  $a_{j1}, a_{j2}, a_{j3}, a_{j4}$  in column  $j$ . To ensure

only legal actions can be selected, a mask  $\mathbf{m}$  is utilized as the selector to enable valid actions and forbid invalid actions.

$$\mathbf{m} = [m_{10}, m_{11}, m_{12}, m_{13}, \dots, m_{2N,0}, m_{2N,1}, m_{2N,2}, m_{2N,3}], \quad (6)$$

where each entry is a binary value. If an action  $a_{ij}$  is valid, the corresponding entry in  $m_{ij}$  is 1. Otherwise, it is 0. In RLMUL, the final masked Q-value vector is the element-wise multiplication of the mask vector and Q-value vector:

$$Q'(s_t) = Q(s_t) \odot \mathbf{m}. \quad (7)$$

Now the decision is given by

$$a_t = \arg \max_a Q'(s_t, a). \quad (8)$$

Note that only non-zero entries are considered. The action applied to column  $j$  changes the number of 3:2 or 2:2 compressors of the current column  $j$ , which may cause the number of compressed PPs of subsequent column  $j+1$  to become 0 or 3. We use the legalization strategy shown in Algorithm 2 to refine the multiplier structure to ensure the PPs are compressed to 2 rows. This strategy sequentially refines from column  $j+1$  to the MSB, addressing under-compression by adding or replacing compressors, and managing over-compression by removing compressors. Similar to the assignment procedure, the legalization process is also deterministic. Under state  $s_t$ , we can get a new state  $s_{t+1}$  after performing action  $a_t$  to modify the structure along with the legalization.

### E. Pareto-driven Reward

In our framework, we define the reward,  $r_t$ , as the improvement in circuit metrics, such as area, delay, and power, achieved by executing an action  $a_t$  at state  $s_t$ . Considering the nature of the trade-off between power, performance, and area (PPA), a superior multiplier design is always expected to achieve Pareto-optimal in terms of these dimensions. To encourage the RL agent to learn to generate Pareto-optimal designs, we introduce a Pareto-driven reward mechanism. This mechanism leverages a synthesis flow under multiple design constraints, enabling the reward to cover a variety of design scenarios: those driven primarily by area, delay, or power, as well as scenarios seeking a trade-off optimization of these three key metrics.

The overall cost metric is calculated as a weighted sum of area, delay, and power, allowing for flexible adjustment of their relative importance in different design scenarios:

$$cost = w_a \sum_{i=1}^n area_i + w_d \sum_{i=1}^n delay_i + w_p \sum_{i=1}^n power_i, \quad (9)$$

where  $area_i$ ,  $delay_i$ , and  $power_i$  are the synthesized metrics under the  $i$ -th constraint.  $w_a$ ,  $w_d$  and  $w_p$  are the weights to trade off PPA. We define our reward  $r$  as the difference between  $s_t$  and  $s_{t+1}$ :

$$r_t = cost_t - cost_{t+1} \quad (10)$$

---

**Algorithm 2** Legalization

---

**Require:** Multiplier structure to be legalized;  $C$ : action column

**Ensure:** Legalized multiplier structure

- 1: **for**  $j \leftarrow (C + 1)$  to  $2N$  **do**
- 2:    $res_j \leftarrow$  Get residual PPs after compression
- 3:   **if**  $res_j = 1$  or  $res_j = 2$  **then**
- 4:     **return** ▷ legalization done
- 5:   **else if**  $res_j == 3$  **then**
- 6:     **if** exists 2:2 comp. in column  $j$  **then**
- 7:       Replace a 2:2 compressor
- 8:     **else**
- 9:       Add a 3:2 compressor
- 10:    **end if**
- 11:   **else if**  $res_j == 0$  **then**
- 12:     **if** exists 2:2 compressor in column  $j$  **then**
- 13:       Delete a 2:2 compressor
- 14:     **else**
- 15:       Delete a 3:2 compressor
- 16:     **end if**
- 17:   **end if**
- 18: **end for**

---

#### F. Training Algorithm

We adopt ResNet-18 [33] as the backbone of Q-Network with the parameters denoted by  $\theta$ . The state undergoes encoding into a tensor representation  $\mathcal{T}$ , as detailed in Section III-B, before being processed by the Q-network. The RL-MUL training methodology, based on the DQN algorithm, is outlined in Algorithm 3. Initially, action selections  $a$  are randomized during the warm-up phase (Line 6), transitioning to policy-based selections in subsequent steps (Line 8). Each iteration  $t$  leads to the transformation of the multiplier’s architecture from  $s_t$  to  $s_{t+1}$ , culminating in a reward  $r_t$  derived from synthesis and timing analysis. This process generates a new transition  $(s_t, a_t, r_t, s_{t+1})$ , which is then added to the replay buffer (Line 12). With the buffer updated, a batch of transitions  $(s', a', r')$  is randomly selected (Line 13) for further processing. The target Q-value for each state-action pair within the batch is determined as follows:

$$y = r' + \gamma \max_{a'} Q(s', a'; \theta), \quad (11)$$

where  $\gamma$  is the discount factor. Based on the expected Q-value  $y$ , a gradient of  $\theta$  can be obtained by:

$$\Delta\theta = \nabla_{\theta}(y - Q(s, a; \theta))^2. \quad (12)$$

Then the network parameter  $\theta$  is updated by gradient descent (Line 14).

## IV. EFFICIENT OPTIMIZATION

Optimizing hardware configurations necessitates an efficient search within a vast design space. Particularly in multiplier design, where an increase in bit width exponentially expands the design space. Therefore, dealing with this enlarged space effectively becomes crucial.

---

**Algorithm 3** RL-MUL flow

---

**Require:**  $\theta_0$ : Initial Q-network parameters;  $M_0$ : initial multiplier structure;  $\gamma$ : discount factor;  $\alpha$ : learning rate;  $T$ : total training steps;  $T_B$ : warm-up steps

**Ensure:**  $\theta$ : Q-network parameters

- 1: Replay buffer  $B \leftarrow \{\}$
- 2: Encode  $s_0$  into  $\mathcal{T}$  based on  $M_0$  ▷ Algorithm 1
- 3:  $t \leftarrow 0$
- 4: **for**  $t \leftarrow 0$  to  $T$  **do**
- 5:   **if**  $t < T_B$  **then**
- 6:      $a_t \leftarrow$  randomly choose from legal actions
- 7:   **else**
- 8:     Get  $a_t$  by Equation (8)
- 9:   **end if**
- 10:   Perform  $a_t$  to  $s_t$  and get  $s_{t+1}$
- 11:   Run EDA tools on  $s_{t+1}$  and get  $r_t$  ▷ Equation (10)
- 12:   Push  $(s_t, a_t, r_t, s_{t+1})$  to  $B$
- 13:   Sample a batch of transitions from  $B$
- 14:   Update  $\theta$  by gradient descent ▷ Equations (11) and (16)
- 15: **end for**

---

In this work, we improve the efficiency of RL-MUL in two perspectives. On one hand, parallel optimization is always a promising solution in this scenario. Their inherent parallelism not only reliably boosts search efficiency but also fosters a thorough exploration of possible designs, enhancing the likelihood of uncovering optimal or nearly optimal solutions. On the other hand, search space pruning is another significant strategy for condensing the design space by discarding less promising designs. This approach emphasizes exploring viable design areas, thus refining the search process and minimizing computational demands. Eliminating inferior designs early on ensures a more targeted and efficient discovery of superior configurations. In addition, integrating metrics with high correlation can achieve a similar purpose, not only significantly simplifying the optimization process, but also enhancing the focus on configurations that genuinely contribute to performance improvements.

#### A. Parallel Agent Training in RL-MUL

Multiple agents running in parallel are more likely to explore different parts of the environment, promoting more efficient and stable policy training. Therefore, we further enhance the proposed framework by training multiple agents in parallel, where each agent is handled by a thread. Following the training stability analysis in [29], each agent in our framework is designed with the A2C scheme, where the policy and value networks share the convolution layers of ResNet-18. Specifically, we employ a shared global network parameter across threads, each interacting with its local environment independently, followed by an average of all threads’ gradient updates to adjust the global parameter.  $n$  parallel threads synchronously process corresponding transitions  $(s_t^{(i)}, a_t^{(i)}, r_t^{(i)}, s_{t+1}^{(i)})$ . Fig. 6 illustrates the synchronous parallel structure with A2C. At each step, given  $n$  is the

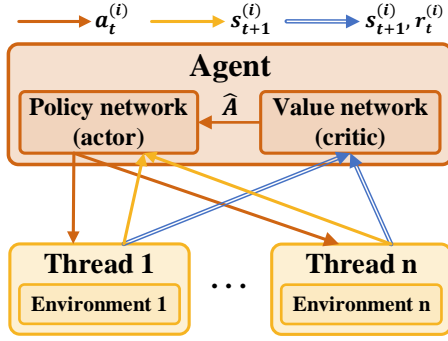


Fig. 6 Synchronous parallel structure in A2C

number of threads, the agent selects  $a_t$  including  $n$  actions for threads, the  $i$ -th thread's environment instance receives its corresponding action  $a_t^{(i)}$  and transitions to the new state  $s_{t+1}^{(i)}$ , which is returned with the reward  $r_t^{(i)}$  to the agent. Thus, in A2C, each element of the transition tuples  $(s_t, a_t, r_t, s_{t+1})$  is an  $n$ -element vector. Then Equation (5) is transformed into:

$$\pi(\cdot|s_t) = [\pi_{11}, \pi_{12}, \pi_{13}, \pi_{14}, \dots, \pi_{2N,1}, \pi_{2N,2}, \pi_{2N,3}, \pi_{2N,4}], \quad (13)$$

where each group of  $\pi_{j1}, \pi_{j2}, \pi_{j3}, \pi_{j4}$  indicates the probability of the four actions  $a_{j1}, a_{j2}, a_{j3}, a_{j4}$  in column  $j$ . The mask is configured as in Section III-D, and the final masked probability distribution vector is:

$$\pi'(\cdot|s_t) = \pi(\cdot|s_t) \odot \mathbf{m}. \quad (14)$$

Now the decision is given by

$$a_t \sim \pi'(\cdot|s_t). \quad (15)$$

Algorithm 4 outlines the parallel training and optimization flow [30], [31]. Firstly,  $n$  threads (Line 1) are initiated. Then, at each step, a multiplier structure alteration  $a_t$  is sampled from Equation (15), which incorporates masks to prevent the selection of actions that lead to invalid multiplier structures (Line 3). Following this, the chosen action is executed to obtain a new structure and its corresponding reward (Line 4). In terms of the model updating, this algorithm employs an  $n$ -step return approach for faster learning, updating the model only when the total training steps constitute an integer multiple of the update interval (Line 5). A policy gradient of  $\theta$  used to update the policy network can be obtained by:

$$\Delta\theta = \nabla_{\theta} \log \pi(a_t|s_t; \theta) \cdot \hat{A}(s_t, a_t), \quad (16)$$

where  $\pi(a_t|s_t; \theta)$  is the policy network defined by parameter  $\theta$  at time  $t$ , and  $\hat{A}$  is the advantage function defined in Equation (4) [32]. Then the policy network parameter  $\theta$  is updated by gradient ascent (Line 6). In addition, the Temporal-Difference (TD) learning [34] aspect of the A2C algorithm guides the value network  $v(s_t; w)$  to converge to the TD target  $y_t$ , defined as:

$$y_t = r_t + \gamma \cdot v(s_{t+1}; w), \quad (17)$$

where  $\gamma$  represents the discount factor. The TD target combines the real reward  $r_t$  after taking the action  $a_t$  with the

---

#### Algorithm 4 RL-MUL flow with multiple threads

---

**Require:**  $n$ : number of threads;  $T$ : total training steps;  $t_{up}$ : update interval

**Ensure:**  $\theta$ : Policy network parameters;  $w$ : value network parameters

- 1: Initialize  $n$  parallel threads
  - 2: **for**  $t \leftarrow 0$  to  $T$  **do**
  - 3: Sample a multiplier structure alteration  $a_t^{(i)}$  by Equation (15),  $\forall i \in \{1, 2, \dots, n\}$
  - 4: Perform  $a_t^{(i)}$  to get structure  $s_{t+1}^{(i)}$  and  $r_t^{(i)}$ ,  $\forall i \in \{1, 2, \dots, n\}$
  - 5: **if**  $t \mid t_{up}$  **then**
  - 6:     Update  $\theta$  by gradient ascent  $\triangleright$  Equation (16)
  - 7:     Update  $w$  by gradient descent  $\triangleright$  Equation (19)
  - 8: **end if**
  - 9: **end for**
- 

predicted value of the next state  $s_{t+1}$ , serving as a crucial element in computing the TD error. This error is expressed as:

$$\delta_t = v(s_t; w) - y_t, \quad (18)$$

measuring the discrepancy between the estimated value of the state before taking the action  $a_t$  and the TD target. In other words, the TD error reflects the accuracy of the value function prediction. Based on the TD error, a gradient of  $w$  used to update the value network can be obtained by:

$$\Delta w = -\nabla_w \frac{(\delta_t)^2}{2} = -\delta_t \cdot \nabla_w v(s_t; w). \quad (19)$$

Then the value network parameter  $w$  is updated by gradient descent (Line 7).

#### B. Objective Space Reduction

The goal of multiplier design space exploration is to find designs that are superior in terms of multiple objectives. In Equation (10), a weighted reward is designed such that the agent can acquire a good trade-off among different objectives, while the selection of weights for each objective can impact the final solutions substantially. The more objectives we have, the more effort is required for tuning the weights. Notably, we investigated a correlation between the area and the power of a multiplier. Based on the architectures we have searched for, it is observed that the power and area are highly correlated. A correlation between these two factors represented by box plots is illustrated in Fig. 7, the upper graph depicts the relationship for 8-bit AND-based multipliers, while the lower plot shows the same for 16-bit AND-based multipliers. The bottom and top boundaries of the box represent the first and third quartiles, respectively, indicating the inter-quartile range (IQR). The median is denoted by the band within the box. The upper whisker represents the maximum value of the data, and the lower whisker represents the minimum value of the data. It can be observed from the trend in Fig. 7 that there exists a strong positive correlation between the area and the power, which suggests that the area is a reliable indicator of the power. Consequently, our methodology gives precedence

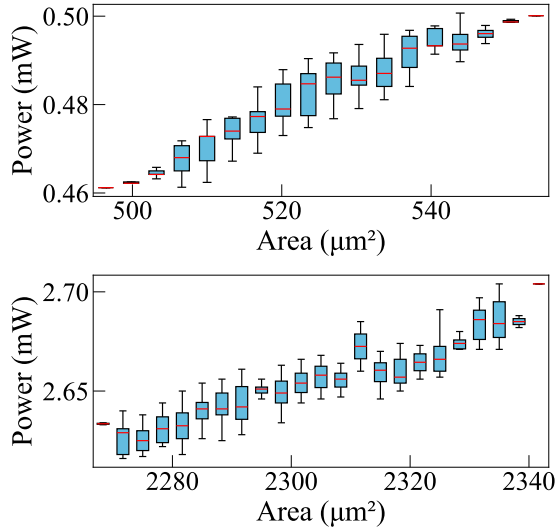


Fig. 7 Correlation between area and power. The upper one is an 8-bit AND-based multiplier, and the lower one is a 16-bit AND-based multiplier.

to area and delay as key optimization metrics, which allows Equation (9) to be further reduced to:

$$cost = w_a \sum_{i=1}^n area_i + w_d \sum_{i=1}^n delay_i \quad (20)$$

### C. Search Space Pruning

Furthermore, another analysis indicates the number of stages of a compressor tree as a significant factor affecting the area and delay of multipliers, as shown in Fig. 8. This analysis takes 8-bit AND-based multiplier structures as an example. Notably, there is a positive relationship between stage number and the parameters of area and delay. This suggests that an increase in stage number is associated with a corresponding rise in these metrics. To mitigate this, our framework integrates a strategy to constrain actions that will lead to excessive stage increases, which facilitates a more efficient search and optimization toward desired multiplier structures.

## V. EXPERIMENTAL RESULTS

### A. Setup

The proposed framework is implemented on a Linux system, powered by a 2.8 GHz AMD EPYC CPU and an NVIDIA RTX 3090 GPU. We use EasyMAC [35] for RTL generation and have extended its capabilities by incorporating Modified Booth Encoding (MBE)-based partial product generation, as well as enhancing support for the RTL generation of merged MAC units. These designs are synthesized using the OpenROAD flow [36] with the NanGate 45nm Open Cell Library [37]. OpenSTA [38] is utilized to perform timing analysis. To ensure the functional correctness of the generated

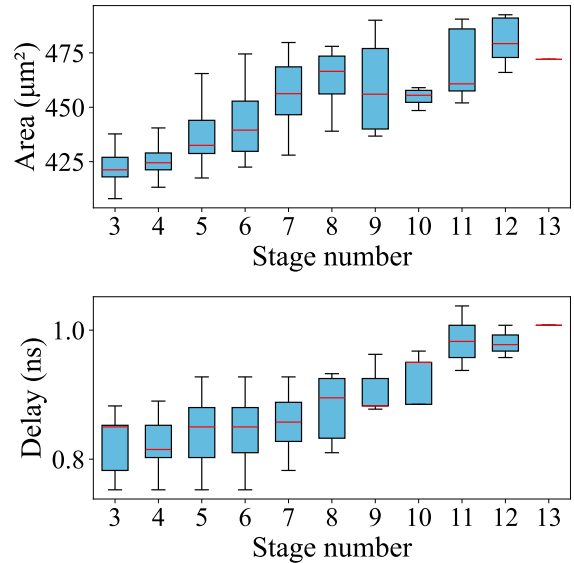


Fig. 8 Correlation between stage number and metrics of 8-bit AND-based multipliers.

multipliers, we first convert RTL into AIGER format using Yosys [39], and use the `cec` command in ABC [40] to perform logic equivalence verification with a golden implementation of multiplier.

Given the prevalent use of 8-bit and 16-bit multipliers, the RL-MUL framework is assessed using both 8-bit and 16-bit multipliers, incorporating AND-based PPG and MBE-based PPG. We compare our approach against established baselines, including the legacy Wallace tree [1], an ILP-based method GOMIL [16], and the simulated annealing (SA) technique. Four delay constraints are configured in Equation (9). The weights  $w_a$  and  $w_d$  range from 0 to 1, resulting in different optimization preferences towards area or delay. In the remaining context, we denote the enhanced and efficient RL-MUL as **RL-MUL-E** to distinguish it from the native implementation of RL-MUL that utilized DQN. In native RL-MUL implementation, we set  $\gamma$  to 0.8,  $\epsilon$  to decay from 0.95 to 0.05, and employ RMSProp optimizer [41] for the training. In the RL-MUL-E implementation, we employ four synchronization threads and a five-step return. We train the original RL-MUL and RL-MUL-E 10000s and run SA for the same amount of time. Synthesizing under varying design constraints produces different netlists for the same RTL design. We synthesize all the obtained multipliers and MACs across target delays from 0.05 ns to 1.2 ns.

Furthermore, to enhance the demonstration of RL-MUL's effectiveness and the performance of the resulting designs, we incorporate these multipliers and MACs from all evaluated methods into large macro designs. Processing Element (PE) arrays, commonly utilized in DNN accelerators, consist of numerous MAC units, making them ideal for evaluating the impact of different multipliers and MACs on area and timing efficiency further. By integrating different multipliers and MACs into PE arrays, specifically following a systolic array



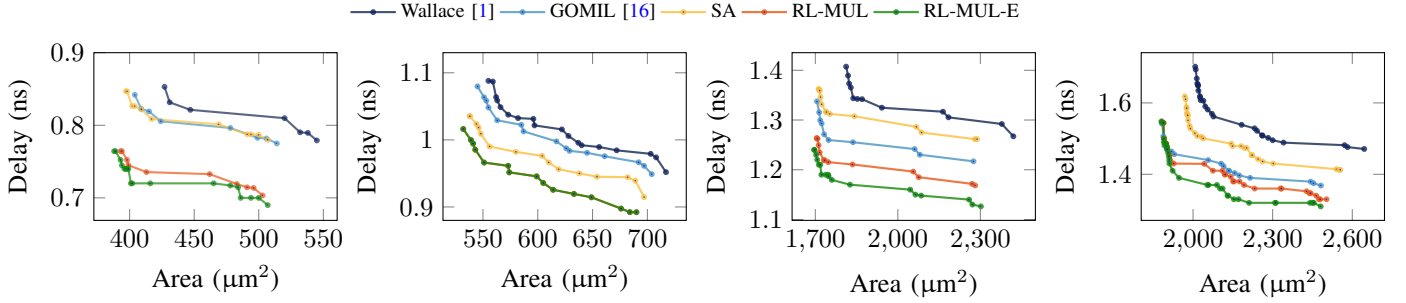


Fig. 9 Pareto-frontiers of the synthesis results on multipliers. From left to right: 8-bit AND-based; 8-bit MBE-based; 16-bit AND-based; 16-bit MBE-based. Note that the Pareto-frontiers of RL-MUL-E and original RL-MUL overlap in the 8-bit MBE-based result.

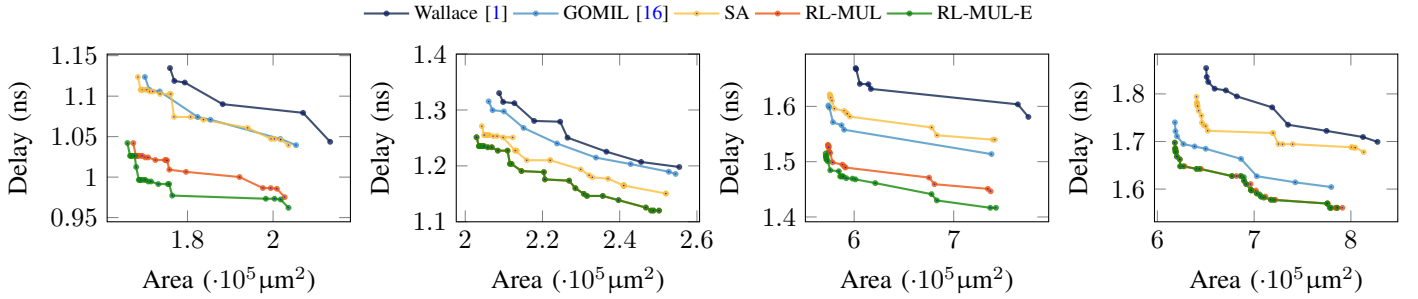


Fig. 10 Pareto-frontiers of the synthesis results on multiplier-implemented PE arrays. From left to right: 8-bit AND-based; 8-bit MBE-based; 16-bit AND-based; 16-bit MBE-based.

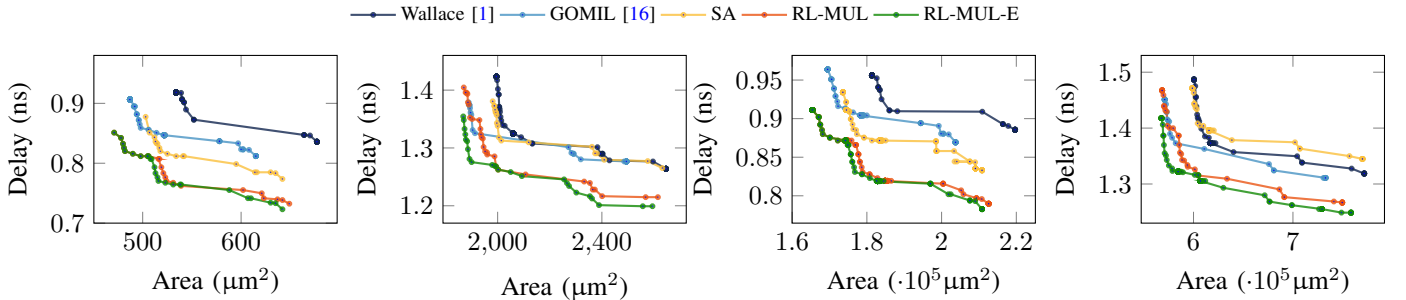


Fig. 11 Pareto-frontiers of the synthesis results on MACs and MAC-implemented PE arrays. From left to right: 8-bit MAC; 16-bit MAC; 8-bit MAC-implemented PE arrays; 16-bit MAC-implemented PE arrays.

architecture, we investigate the potential for improvements in both area and timing within these structures.

### B. Multiplier Performance Comparison

The resulting area-delay curves for multipliers are illustrated in Fig. 9, where the designs derived from the RL-MUL framework outperform all baselines. Detailed statistics of minimum area, delay, and balanced area-delay metrics are presented in TABLE I (the optimal results are marked in bold) for multipliers. Through the RL-MUL framework, we achieve up to 10.0% area reduction under the minimum area constraint and a 12.5% decrease in delay under the minimum delay constraint. Additionally, the implementation

in PE arrays, as shown in Fig. 10 and TABLE II, indicates similar performance, with up to a 6.0% area reduction and up to 11.5% delay decrease.

The hypervolume [42], which measures the volume enclosed by the Pareto frontier and a reference point in the objective space, to evaluate the quality of the Pareto frontiers, as depicted in Fig. 13. Hypervolume comparisons for multipliers presented in Fig. 14(a) show that RL-MUL generates significantly larger hypervolume than GOMIL, with average increases of 85.9%. RL-MUL-E shows an improvement of 11.1% compared to the original RL-MUL. Similarly, for PE arrays constructed with the multiplier, as shown in Fig. 14(b), the average improvement of RL-MUL-E compared

TABLE I Multiplier area and timing comparison.

Preference	Method	8-bit				16-bit			
		AND		MBE		AND		MBE	
		Area ( $\mu\text{m}^2$ )	Delay (ns)	Area ( $\mu\text{m}^2$ )	Delay (ns)	Area ( $\mu\text{m}^2$ )	Delay (ns)	Area ( $\mu\text{m}^2$ )	Delay (ns)
Area	Wallace [1]	427	0.8530	555	1.0880	1812	1.4073	2008	1.7016
	GOMIL [16]	404	0.8420	545	1.0797	1706	1.3375	1882	1.5432
	SA	397	0.8468	538	1.0353	1712	1.3619	1969	1.6184
	<b>RL-MUL</b>	393	0.7643	<b>532</b>	<b>1.0162</b>	1705	1.2633	1882	1.5478
	<b>RL-MUL-E</b>	<b>388</b>	<b>0.7643</b>	<b>532</b>	<b>1.0162</b>	<b>1696</b>	<b>1.2481</b>	<b>1881</b>	<b>1.5478</b>
Timing	Wallace [1]	545	0.7791	720	0.9601	2420	1.2672	2645	1.4709
	GOMIL [16]	514	0.7750	706	0.9571	2281	1.2169	2482	1.3684
	SA	507	0.7800	697	0.9147	2280	1.2616	2551	1.4125
	<b>RL-MUL</b>	503	0.7033	<b>690</b>	<b>0.8922</b>	2281	1.1684	2475	1.3318
	<b>RL-MUL-E</b>	<b>507</b>	<b>0.6931</b>	<b>690</b>	<b>0.8922</b>	<b>2302</b>	<b>1.1263</b>	<b>2481</b>	<b>1.3085</b>
Trade-off	Wallace [1]	458	0.8328	637	1.0018	2184	1.3054	2300	1.4954
	GOMIL [16]	435	0.8086	629	0.9837	2061	1.2416	2106	1.4298
	SA	402	0.8265	556	0.9901	1738	1.3161	2016	1.5071
	<b>RL-MUL</b>	399	0.7451	<b>551</b>	<b>0.9662</b>	1731	1.2192	1927	1.4339
	<b>RL-MUL-E</b>	<b>401</b>	<b>0.7252</b>	<b>551</b>	<b>0.9662</b>	<b>1722</b>	<b>1.1875</b>	<b>1947</b>	<b>1.3923</b>

TABLE II PE array (multiplier) area and timing comparison.

Preference	Method	8-bit				16-bit			
		AND		MBE		AND		MBE	
		Area ( $\mu\text{m}^2$ )	Delay (ns)	Area ( $\mu\text{m}^2$ )	Delay (ns)	Area ( $\mu\text{m}^2$ )	Delay (ns)	Area ( $\mu\text{m}^2$ )	Delay (ns)
Area	Wallace [1]	175892	1.1347	208782	1.3302	601492	1.6693	650385	1.8543
	GOMIL [16]	170036	1.1237	206058	1.3154	574117	1.6017	618107	1.7403
	SA	168401	1.1237	204288	1.2711	575479	1.6216	640443	1.794
	<b>RL-MUL</b>	167312	1.0421	<b>202926</b>	<b>1.2512</b>	573709	1.5305	618107	1.6976
	<b>RL-MUL-E</b>	<b>165950</b>	<b>1.0421</b>	<b>202926</b>	<b>1.2512</b>	<b>571394</b>	<b>1.5148</b>	<b>617971</b>	<b>1.6976</b>
Timing	Wallace [1]	213345	1.0436	258016	1.1988	775001	1.5809	827503	1.6992
	GOMIL [16]	205378	1.0395	254475	1.1856	739591	1.5137	785896	1.6085
	SA	203607	1.0395	251955	1.1505	739318	1.5398	813339	1.6777
	<b>RL-MUL</b>	202722	0.9752	<b>250185</b>	<b>1.1200</b>	737139	1.4464	<b>778678</b>	<b>1.5607</b>
	<b>RL-MUL-E</b>	<b>203607</b>	<b>0.9621</b>	<b>250185</b>	<b>1.1200</b>	<b>736731</b>	<b>1.4166</b>	<b>778269</b>	<b>1.5607</b>
Trade-off	Wallace [1]	191214	1.1017	236566	1.2254	628322	1.6419	735028	1.7352
	GOMIL [16]	185357	1.0709	221857	1.2703	600947	1.5727	649908	1.6847
	SA	169014	1.1079	2,04901	1.2552	580110	1.5959	652019	1.7225
	<b>RL-MUL</b>	167925	1.0263	<b>203539</b>	<b>1.2353</b>	578339	1.4987	623691	1.6479
	<b>RL-MUL-E</b>	<b>168606</b>	<b>0.9966</b>	<b>203539</b>	<b>1.2353</b>	<b>576024</b>	<b>1.4844</b>	<b>623555</b>	<b>1.6479</b>

TABLE III MAC and PE array (MAC) area and timing comparison.

Preference	Method	MAC				PE-MAC			
		8-bit		16-bit		8-bit		16-bit	
		Area ( $\mu\text{m}^2$ )	Delay (ns)	Area ( $\mu\text{m}^2$ )	Delay (ns)	Area ( $\mu\text{m}^2$ )	Delay (ns)	Area ( $\mu\text{m}^2$ )	Delay (ns)
Area	Wallace [1]	534	0.9182	639	1.1749	181340	0.9561	600471	1.4868
	GOMIL [16]	487	0.9063	603	1.1153	169491	0.9638	571053	1.451
	SA	503	0.8775	615	1.1047	173577	0.9342	598836	1.4714
	<b>RL-MUL</b>	<b>471</b>	<b>0.8511</b>	607	1.0611	165405	0.9112	568465	1.4673
	<b>RL-MUL-E</b>	<b>471</b>	<b>0.8511</b>	<b>601</b>	<b>1.0611</b>	<b>165405</b>	<b>0.9112</b>	<b>567784</b>	<b>1.4178</b>
Timing	Wallace [1]	677	0.8359	821	1.0834	219678	0.8856	771664	1.3187
	GOMIL [16]	615	0.8119	720	1.0216	203743	0.8693	730670	1.3109
	SA	642	0.7737	716	1.0215	210825	0.8331	769893	1.3448
	<b>RL-MUL</b>	649	0.7324	723	0.9462	212596	0.7897	749533	1.2668
	<b>RL-MUL-E</b>	<b>642</b>	<b>0.7231</b>	<b>718</b>	<b>0.9462</b>	<b>210825</b>	<b>0.7827</b>	<b>758385</b>	<b>1.2487</b>
Trade-off	Wallace [1]	552	0.8727	650	1.1362	186038	0.9107	611502	1.3851
	GOMIL [16]	498	0.859	614	1.0714	172283	0.9161	582085	1.3729
	SA	518	0.8202	626	1.0739	177322	0.8799	604148	1.4084
	<b>RL-MUL</b>	<b>482</b>	<b>0.8202</b>	618	1.0129	168197	0.8799	588486	1.3429
	<b>RL-MUL-E</b>	<b>482</b>	<b>0.8202</b>	<b>612</b>	<b>1.0129</b>	<b>176777</b>	<b>0.8309</b>	<b>578816</b>	<b>1.3233</b>

with GOMIL and original RL-MUL is 96.1% and 8.4% respectively.

### C. MAC Performance Comparison

The curves in Fig. 11 for MACs and PE arrays consisting of MAC, along with the detailed comparisons in TABLE III, demonstrate that RL-MUL designs achieve superior performance compared to baselines. The RL-MUL framework leads

to up to a 13.4% area reduction under the minimum area constraint and a 15.6% decrease in delay under the minimum delay constraint for MACs. Similarly, PE arrays benefit from up to a 9.6% reduction in area and a 13.1% decrease in delay.

The hypervolume metrics, shown in Fig. 14(c) for MACs and PE arrays implemented by MAC, highlight RL-MUL's efficiency. RL-MUL generates an average of 81.7% more hypervolume than GOMIL for MACs and 80.9% for the

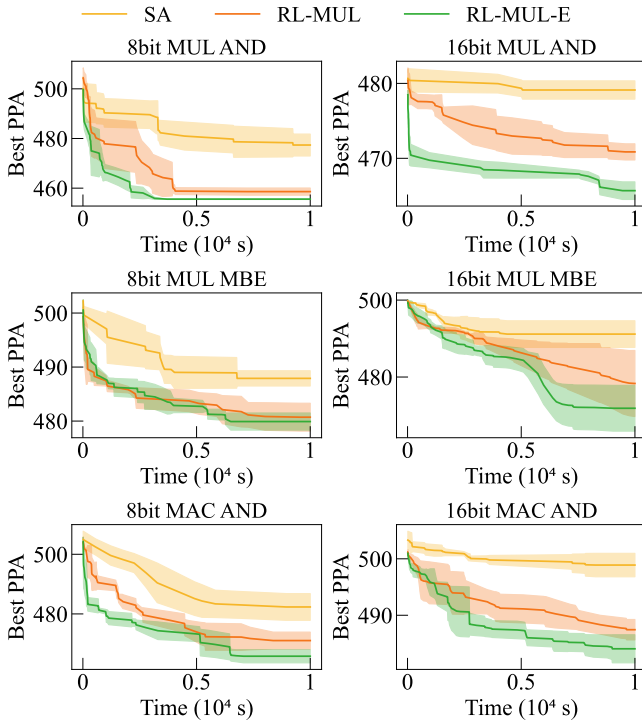


Fig. 12 Optimization trajectories for different methods illustrate the mean PPA  $\pm$  standard error. The shaded areas represent the standard deviation of the PPA values.

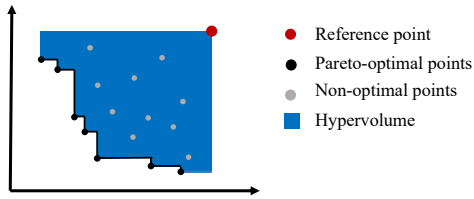


Fig. 13 An illustration of hypervolume. In our problem, a larger hypervolume is better.

arrays. When comparing the performance of RL-MUL-E to the original RL-MUL, there is a 7.0% increase for MACs and a 7.9% increase for arrays.

Regardless of the multiplier cases or the MAC cases, it is observed that the advantage of RL-MUL over the SA approach varies between 8-bit and 16-bit configurations. GOMIL outperforms SA in larger bit widths, suggesting that evolutionary algorithms may struggle with large design spaces due to their complexity. The improvement margins over the SA method vary between 8-bit and 16-bit designs, with GOMIL outperforming SA in larger bit widths. This suggests the evolutionary algorithm’s limitations in addressing the expansive design space of larger bit widths. Additionally, the ILP-based method GOMIL simplifies the cost function by focusing solely on the area as the optimization objective. This approach limits its ability to consistently achieve optimization gains in terms of delay. In contrast, our approach employs multi-objective optimization, allowing us to attain Pareto-optimal results across both area and delay, demonstrating RL-

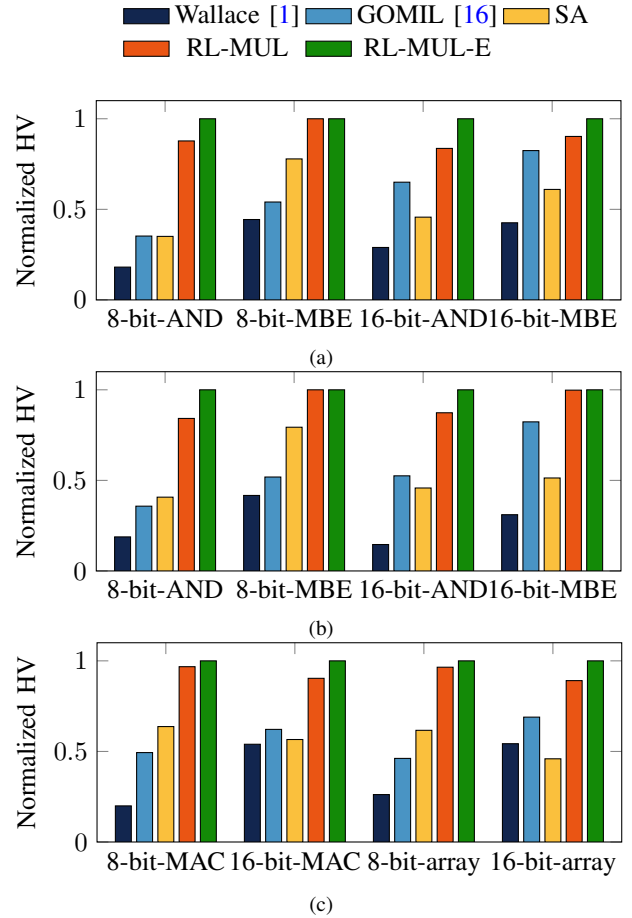


Fig. 14 Pareto-frontiers hypervolume comparison of (a) multipliers; (b) multiplier-implemented PE arrays (c) MACs and MAC-implemented PE arrays.

MUL’s consistent superiority across evaluations.

#### D. Efficient and Stable Training

We conducted six experiments on the original RL-MUL, RL-MUL-E, and SA algorithms, with a fixed PPA weight across two bit-widths. These experiments are categorized into three groups: one focusing on AND-based MUL operations, another on MUL operations employing Booth encoding, and a third on MAC operations. The mean PPA results are represented by a solid line, with the standard deviation depicted as the surrounding shadow in Fig. 12. Across all datasets, our RL methods consistently demonstrate superior performance, significantly outperforming SA. Particularly, the RL-MUL-E demonstrates superior results and a more stable and efficient training process.

## VI. CONCLUSION

In this research, we introduce RL-MUL, a novel framework for optimizing multipliers through reinforcement learning. The framework utilizes an RL agent that adapts based on EDA tool feedback to engineer multipliers achieving Pareto optimality. We demonstrate that RL-MUL can design multipliers and MACs that Pareto-dominate multipliers produced

by existing approaches. The obtained optimized multiplier and MACs can be further applied in the implementation of a larger module such as a PE array. Looking ahead, we aim to broaden the application of our RL methodology to encompass more extensive datapath components, enhancing the scope and impact of our optimization efforts.

## REFERENCES

- [1] C. S. Wallace, "A suggestion for a fast multiplier," *IEEE Transactions on Electronic Computers*, vol. EC-13, no. 1, pp. 14–17, 1964.
- [2] P. Stelling and V. Oklobdzija, "Implementing multiply-accumulate operation in multiplication time," in *Proceedings 13th IEEE Symposium on Computer Arithmetic*, 1997, pp. 99–106.
- [3] L. Dadda, "Some schemes for fast serial input multipliers," in *1983 IEEE 6th Symposium on Computer Arithmetic (ARITH)*, 1983, pp. 52–59.
- [4] J. Fadavi-Ardekani, "M\*n booth encoded multiplier generator using optimized wallace trees," *IEEE Transactions on Very Large Scale Integration Systems (TVLSI)*, vol. 1, no. 2, pp. 120–125, June 1993.
- [5] N. Itoh, Y. Tsukamoto, T. Shibagaki, K. Nii, H. Takata, and H. Makino, "A 32/spl times/24-bit multiplier-accumulator with advanced rectangular styled wallace-tree structure," in *IEEE International Symposium on Circuits and Systems (ISCAS)*, 2005, pp. 73–76 Vol. 1.
- [6] K. Bickerstaff, M. Schulte, and E. Swartzlander, "Reduced area multipliers," in *Proceedings of International Conference on Application Specific Array Processors (ASAP '93)*, 1993, pp. 478–489.
- [7] X.-V. Luu, T.-T. Hoang, T.-T. Bui, and A.-V. Dinh-Duc, "A high-speed unsigned 32-bit multiplier based on booth-encoder and wallace-tree modifications," in *2014 International Conference on Advanced Technologies for Communications (ATC 2014)*, 2014, pp. 739–744.
- [8] C.-W. Tung and S.-H. Huang, "A high-performance multiply-accumulate unit by integrating additions and accumulations into partial product reduction process," *IEEE Access*, vol. 8, pp. 87367–87377, 2020.
- [9] S. Zhang, J. Gu, S. Yin, L. Liu, and S. Wei, "A multiple-precision multiply and accumulation design with multiply-add merged strategy for ai accelerating," in *2021 26th Asia and South Pacific Design Automation Conference (ASP-DAC)*, 2021, pp. 229–234.
- [10] N. Shavit, I. Stanger, R. Taco, M. Lanuzza, and A. Fish, "A 0.8-v, 1.54-pj/940-mhz dual-mode logic-based 16x16-b booth multiplier in 16-nm finfet," *IEEE Solid-State Circuits Letters*, vol. 3, pp. 314–317, 2020.
- [11] D. Jangalwa, M. Nagabushanam, and M. C. Parameshwara, "Design and analysis of 8-bit multiplier for low power vlsi applications," in *2022 IEEE 2nd Mysore Sub Section International Conference (MysuruCon)*, 2022, pp. 1–5.
- [12] D. B. R. D. Shylu Sam, M. G. D. Jayanthi, S. I. J. S. Babafakruddin, and S. E. G. V., "Design of low power pass transistor logic based adders for multiplier in 90nm cmos process," in *2023 4th International Conference on Signal Processing and Communication (ICSPC)*, 2023, pp. 206–210.
- [13] V. Oklobdzija, D. Villegier, and S. Liu, "A method for speed optimized partial product reduction and generation of fast parallel multipliers using an algorithmic approach," *IEEE Transactions on Computers*, vol. 45, no. 3, pp. 294–306, 1996.
- [14] C. Martel, V. Oklobdzija, R. Ravi, and P. Stelling, "Design strategies for optimal multiplier circuits," in *Proceedings of the 12th Symposium on Computer Arithmetic*, 1995, pp. 42–49.
- [15] P. Stelling, C. Martel, V. Oklobdzija, and R. Ravi, "Optimal circuits for parallel multipliers," *IEEE Transactions on Computers*, vol. 47, no. 3, pp. 273–285, 1998.
- [16] W. Xiaol, W. Qian, and W. Liu, "Gomil: Global optimization of multiplier by integer linear programming," pp. 374–379, 2021.
- [17] J. Liu, Y. Zhu, H. Zhu, C.-K. Cheng, and J. Lillis, "Optimum prefix adders in a comprehensive area, timing and power design space," in *IEEE/ACM Asia and South Pacific Design Automation Conference (ASPDAC)*, 2007, pp. 609–615.
- [18] J. Liu, S. Zhou, H. Zhu, and C.-K. Cheng, "An algorithmic approach for generic parallel adders," in *IEEE/ACM International Conference on Computer-Aided Design (ICCAD)*, 2003, pp. 734–740.
- [19] S. Roy, M. Choudhury, R. Puri, and D. Z. Pan, "Towards optimal performance-area trade-off in adders by synthesis of parallel prefix structures," in *ACM/IEEE Design Automation Conference (DAC)*, 2013, pp. 1–8.
- [20] H. Parandeh-Afshar, P. Brisk, and P. Jenne, "Efficient synthesis of compressor trees on fpgas," in *2008 Asia and South Pacific Design Automation Conference*, 2008, pp. 138–143.
- [21] H. Parandeh-Afshar, A. Neogy, P. Brisk, and P. Jenne, "Compressor tree synthesis on commercial high-performance fpgas," *ACM Trans. Reconfigurable Technol. Syst.*, vol. 4, no. 4, dec 2011.
- [22] M. Kumm and J. Kappauf, "Advanced compressor tree synthesis for fpgas," *IEEE Transactions on Computers*, vol. 67, no. 8, pp. 1078–1091, 2018.
- [23] H. Geng, Y. Ma, Q. Xu, J. Miao, S. Roy, and B. Yu, "High-speed adder design space exploration via graph neural processes," *IEEE Transactions on Computer-Aided Design of Integrated Circuits and Systems (TCAD)*, vol. 41, no. 8, pp. 2657–2670, 2022.
- [24] Y. Ma, S. Roy, J. Miao, J. Chen, and B. Yu, "Cross-layer optimization for high speed adders: A pareto driven machine learning approach," *IEEE Transactions on Computer-Aided Design of Integrated Circuits and Systems (TCAD)*, vol. 38, no. 12, pp. 2298–2311, 2019.
- [25] R. Roy, J. Raiman, N. Kant, I. Elkin, R. Kirby, M. Siu, S. Oberman, S. Godil, and B. Catanzaro, "Prefixrl: Optimization of parallel prefix circuits using deep reinforcement learning," in *ACM/IEEE Design Automation Conference (DAC)*, 2021, pp. 853–858.
- [26] H. Wang, K. Wang, J. Yang, L. Shen, L. Sun, H.-S. Lee, and S. Han, "Gcn-rl circuit designer: Transferable transistor sizing with graph neural networks and reinforcement learning," in *ACM/IEEE Design Automation Conference (DAC)*, 2020.
- [27] N. Siddharth, P. Geraldo, H. Corey, T. Yang, K. Brucek, and H. Ren, "Transsizer: A novel transformer-based fast gate sizer," in *IEEE/ACM International Conference on Computer-Aided Design (ICCAD)*, 2022.
- [28] R. Bellman, "Dynamic programming," *Science*, vol. 153, no. 3731, pp. 34–37, 1966.
- [29] V. Mnih, A. P. Badia, et al., "Asynchronous Methods for Deep Reinforcement Learning," in *International Conference on Machine Learning (ICML)*, vol. 48, 2016, pp. 1928–1937.
- [30] P. Winder, *Reinforcement learning*. O'Reilly Media, 2020.
- [31] M. Sewak, *Deep reinforcement learning*. Springer, 2019.
- [32] V. Mnih, A. P. Badia, M. Mirza, A. Graves, T. Lillicrap, T. Harley, D. Silver, and K. Kavukcuoglu, "Asynchronous methods for deep reinforcement learning," in *International conference on machine learning*. PMLR, 2016, pp. 1928–1937.
- [33] K. He, X. Zhang, S. Ren, and J. Sun, "Deep residual learning for image recognition," in *IEEE Conference on Computer Vision and Pattern Recognition (CVPR)*, 2016, pp. 770–778.
- [34] J. Peng and R. J. Williams, "Incremental multi-step Q-learning," in *Machine Learning Proceedings 1994*. Elsevier, 1994, pp. 226–232.
- [35] J. Zhang, Q. Gao, Y. Guo, B. Shi, and G. Luo, "Easymac: Design exploration-enabled multiplier-accumulator generator using a canonical architectural representation," in *IEEE/ACM Asia and South Pacific Design Automation Conference (ASPDAC)*, 2022, pp. 647–653.
- [36] T. Ajayi, D. Blaauw, T. Chan, C. Cheng, V. Chhabria, D. Choo, M. Coltella, S. Dobre, R. Dreslinski, M. Fogaça et al., "Openroad: Toward a self-driving, open-source digital layout implementation tool chain," *Proc. GOMACTECH*, pp. 1105–1110, 2019.
- [37] Nangate Inc., "Open Cell Library v2008\_10 SP1," 2008. [Online]. Available: <http://www.nangate.com/openlibrary/>
- [38] Parallax Software Inc., "OpenSTA," <https://github.com/The-OpenROAD-Project/OpenSTA>.
- [39] C. Wolf, "Yosys open synthesis suite," <https://yosyshq.net/yosys/>.
- [40] Berkeley Logic Synthesis and Verification Group, "ABC: A System for Sequential Synthesis and Verification," <http://www.eecs.berkeley.edu/~alanmi/abc/>.
- [41] Geoff Hinton, "RMSProp," [https://www.cs.toronto.edu/~tijmen/csc321/slides/lecture\\_slides\\_lec6.pdf](https://www.cs.toronto.edu/~tijmen/csc321/slides/lecture_slides_lec6.pdf).
- [42] E. Zitzler, D. Brockhoff, and L. Thiele, "The hypervolume indicator revisited: On the design of pareto-compliant indicators via weighted integration," in *International Conference on Evolutionary Multi-Criterion Optimization*. Springer, 2007, pp. 862–876.